2009 American Control Conference
Hyatt Regency Riverfront, St. Louis, MO, USA
June 10-12, 2009

Stability of Potential Function Formation Control with Communication and Processing Delay

Luke M. Wachter and Laura E. Ray, *Member, IEEE*

***Abstract*— We derive conditions for which a circular formation of nonholonomic robots under potential function control is stable, where robots assume a radially-directed pose at equilibrium. In addition to the delay-free case, we investigate the stability of the equilibrium when communication and local processing introduce delay. It is shown that while sufficiently large processing delay always leads to instability, with the right choice of control parameters, the system can tolerate unbounded communication delay. The analytical results are compared with simulations of a fleet of nonholomonic robots as well as with experimental data.**

I. Introduction

Applications for mobile robot pattern formation are broad. In many cases, formation control is a prerequisite for higher level tasks, such as manipulation [1] and distributed sensing [2]. Various approaches to formation control have been developed, including consensus approaches and leader-follower hierarchies [3-6]. In both cases, a target formation is explicitly encoded in a constraint graph. In contrast, artificial potential function (APF) control does not specify a formation explicitly but rather drives the robots down the gradient of a potential field such that a formation, shaped by choice of the potential, emerges at global or local minima [7-9]. Ad hoc formation emergence has several benefits: It allows for spontaneous addition of vehicles; it makes the formation robust to vehicle failure; and it enables each robot to claim any place in the formation. It is homogeneous, since no unique assignment in a constraint graph is needed.

Guaranteeing stability is a key challenge in formation control and is addressed in the literature [3-5,7,9]. However, few papers address the effects of delay [10], which is ubiquitous in physical systems, and fewer still consider delay in systems of nonholonomic robots. Example papers that consider delay include [11] who extend the notion of string stability to include delay due to propagation of information through a string of platooning vehicles and [5], which presents exact bounds on tolerable delay in a system of first-order agents with first order dynamics. All information, both local and communicated, is assumed to be delayed equally. [12] generalizes these results to determine bounds on uniform time-varying delays, and non-uniform constant, or time-varying delays for preserving average consensus. [13] examines how delay in processing sensor data leads to instability in nonholonomic robots under APF control, albeit for a single robot case.

Lyapunov's direct method is typically used to study stability of APF methods since potential functions are natural Lyapunov functions [7-9,13]. Unfortunately, this approach is not easily extended to systems with delay. We use Lyapunov's indirect method to investigate local stability of an equilibrium state in a nonholonomic system in the presence of delay. We distinguish between local processing delay due to computation for sensor fusion and control, and communication delay due to information exchange. Since only a subset of information is subject to communication delay, its effects are distinct from those of processing lag.

APF control accommodates the needs of a differential-steered four-wheel drive robot called the Dynabot [14,15]. We study a group of n such robots coming into a circular formation about a target and assuming a radially-directed pose at equilibrium, a formation of interest for certain distributed sensing tasks (e.g., acoustic sensor arrays). Dynabots use GPS and inertial measurements to track their location. Each robot communicates position to neighboring robots. High speed navigation (up to 10 m/s) and low-cost components are stipulated. The radial-basis APF controller of [8] is adopted because of its computational simplicity and need for only position information for each robot.

The unique dynamics of nonholonomic robots about a circular equilibrium give rise to a circulant system Jacobian. We use properties of circulant matrices to derive exact limits on tolerable communication and processing delay. While we consider only circular equilibrium, the paper provides a step towards characterizing delay effects in nonholonomic multi-robot systems, and specifically, the relative effects of communication delay vs. local processing delay. Such results may inform system design in terms of information to be communicated vs. decentralized sensing. Analytical findings are compared with full nonlinear simulations of the multi-robot system, as well as with experimental data.

II. Potential Function Control

The APF controller consists of radial intra-robot potentials centered at each agent and virtual leader potentials that attract the fleet to a target and shape the formation [8]. The total potential is the sum of the virtual leader and the intra-robot potentials. The potential maintains separation between robots while driving the fleet toward the virtual leader. The intra-robot potential due to robot j, V_{dj}, is

$$V_{dj} = \alpha_d \left[\ln(d_j) + \frac{d_0}{d_j} \right]. \quad (1)$$

d_j is the radial distance from robot j, d_0 is the distance at which the potential is minimized and α_d is a gain. Figure 1 shows the normalized APF. Similarly, the virtual leader potential V_h is given by

$$V_h = \alpha_h \left[\ln(d) + \frac{h_0}{d} \right]. \quad (2)$$

d is the radial distance from the virtual leader. h_0 and α_h are the distance at which the potential is minimized and controller gain, respectively. The magnitude of the control

This research is supported by NIST under Grant No. 60NANB4D1144 and by the Army Research Office under contract No W911NF- 06-1-0153.

Luke M. Wachter was with the Thayer School of Engineering, Dartmouth College.

Laura E. Ray. is with the Thayer School of Engineering, Dartmouth College 603-646-1243 (e-mail: lray@dartmouth.edu).

force F_{ij} exerted on any robot *i* due to the potential centered at robot *j* is given by the negative gradient of V_{dj} at the location of robot *i*

$$F_{ij} = -\alpha_d \left[\frac{1}{d_{ij}} - \frac{d_0}{d_{ij}^2} \right] \quad (3)$$

where d_{ij} is the distance between robots *i* and *j*. The force on robot *i* due to the virtual leader is

$$F_i = -\alpha_h \left[\frac{1}{d_i} - \frac{h_0}{d_i^2} \right]. \quad (4)$$

d_i is the distance of robot *i* from the virtual leader. We limit our investigation to the case of a single virtual leader.

To use this control law, robots must know the positions of all other robots and the position of the virtual leader. The static virtual leader position is assigned at runtime. Positions of neighboring robots are communicated. Regardless of the communication protocol, delay is introduced by communication. Dynabots use all-to-all broadcast over an ad-hoc 802.11.b wireless network to exchange position information; since the number of robots is small, broadcast is appropriate. The communication latency is found to fit a Poisson distribution, which is modeled empirically as a function of message size *N* and number of robots communicating *n* for $n \le 7$ [15]. Figure 2 shows the resulting cumulative probability of receiving a message after a certain time, with an RCM3100 processor, and $N = 58$ bytes, the size of the state message the Dynabots exchange.

The Dynabot's longitudinal and lateral dynamics in body-fixed coordinates are given by

$$m\dot{v}_x = F_{Rx} + F_{Lx} - R_x - Dv_x + m\dot{\phi}v_y \quad (6)$$
$$m\dot{v}_y = -R_y - m\dot{\phi}v_x \quad (7)$$

where v_x, v_y are longitudinal and lateral velocities in body-fixed axes, $\dot{\phi}$ is the yaw rate, F_{Rx}, F_{Lx} are applied forces that result from application of torque to the wheel on the left and right sides, R_x, R_y are resistance forces, *m* is the vehicle mass, and *D* is a damping coefficient. Resistance forces are modeled as Coulomb friction up to some maximum friction force as described in [16]. We assume longitudinal slip is negligible, such that F_{Rx}, F_{Lx} are derived directly from applied torques. The mapping between the APF commanded force and wheel torques is addressed in [16] and includes local longitudinal controllers for steering and braking that enable the vehicle to match the commanded APF force. The local controller includes a damping term Cv_x. In [16] the natural resistance in the longitudinal direction is found to consist of constant rolling resistance and viscous damping. Since linear models are assumed here, Dv_x in eq. 6 encompasses both of these terms. However, the natural damping is small such that $C > D$, thus we assume $D = 0$ for the subsequent analysis. We consider the case $D \neq 0$ in section VII.

III. Existence of a Circular Equilibrium

We first establish that the circular configuration about the virtual leader is an equilibrium state.

Theorem 1. *The configuration of robots equally spaced around a circle of radius r_0 centered at the virtual leader is an equilibrium for the controller of section II, for all $n > 0$.*

Proof. Consider *n* robots under APF control as in Fig. 3. At equilibrium, each robot is distance r_0 from the virtual leader

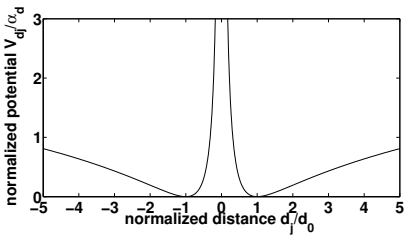

Figure 1. Normalized profile of the artificial potential function.

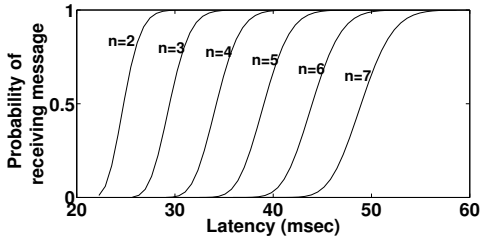

Figure 2. Cumulative probability of receiving a message after a certain delay using Dynabot processor for n = 2 to 7 and N = 58.

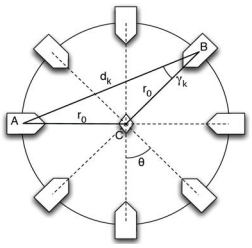

Figure 3. Definition diagram of circular equilibrium with radial pose.

with angle $\theta = 2\pi/n$ between robots. The *i* th robot, *j* th robot (*k* robots away from robot *i*) and virtual leader form an isosceles triangle with side r_0, and base d_k, where d_k is the distance between any two robots *k* robots apart. Since robots are evenly spaced by θ, $\angle ACB = k\theta$, and $\gamma_k = (\pi - k\theta)/2$ is the angle between any two robots *k* robots apart. $d_k = r_0 \sin(k\theta) / \sin(\frac{\pi}{2} - k\theta/2)$ is found by the Law of Sines, which using trigonometric identities, reduces to $d_k = 2r_0 \sin(\phi_k)$ where $\phi_k = k\pi/n$. Therefore, at equilibrium, the magnitude of the force on any two robots *k* robots apart is

$$F(k) = \alpha_d \left(\frac{1}{2r_0 \sin(\phi_k)} - \frac{d_0}{4r_0^2 \sin^2(\phi_k)} \right) \quad (8)$$

By symmetry, tangential force components cancel. The radial force component is of interest in finding r_0. It is given by

$$F_r(k) = F(k)\cos(\gamma_k) = F(k)\sin(\phi_k) = \alpha_d \left(\frac{1}{2r_0} - \frac{d_0}{4r_0^2 \sin(\phi_k)} \right) \quad (9)$$

At equilibrium, the sum of all forces on a robot must equal zero, i.e., $0 = \alpha_d \sum_{k=1}^{n-1} \left(1/(2r_0) - d_0/\left(4r_0^2 \sin(\phi_k)\right) \right) + \alpha_h \left(1/r_0 - h_0/r_0^2 \right)$.

This gives $r_0 = \left[\sum_{k=1}^{n-1} \frac{d_0}{4\sin(\phi_k)} + h_0 \frac{\alpha_h}{\alpha_d} \right] \Big/ \left[\frac{n-1}{2} + \frac{\alpha_h}{\alpha_d} \right]$, which is always positive for positive APF parameters and $n > 0$. Therefore, an equilibrium configuration always exists in which the robots are evenly spaced about a circle of radius r_0 centered at the virtual leader.

Since the robots experience attractive control forces at equilibrium, the formation compresses so that $r_0 < h_0$. To

simplify, we normalize parameters as $\alpha* = \alpha_h / \alpha_d$ and $h_0^* = h_0 / d_0$. The dimensionless equilibrium $r_0^* = r_0 / d_0$ is

$$r_0^* = \frac{\left[\sum_{k=1}^{n-1} \frac{1}{4\sin(\phi_k)} + h_0^* \alpha^*\right]}{\left[\frac{n-1}{2} + \alpha^*\right]} \tag{10}$$

In general, r_0^* increases with h_0^*. For large values of h_0^*, increasing α^* also tends to expand the equilibrium radius, however for small h_0^*, increasing α^* has the opposite effect.

IV. Linearization about the Circular Equilibrium

Stability of the circular equilibrium is investigated using Lyapunov's indirect method. The linearized system is derived for the configuration of robots depicted in Fig. 3. Compared to the open field, the region near equilibrium is a bottleneck where robots are forced into close proximity and the control sensitivity to robot position is high. As a result, the system dynamics close to equilibrium are interesting.

For linearization, we assume 1) robots are homogeneous, and 2) robots behave as radially-constrained point masses around the equilibrium state. Constraining motion acknowledges that the physical robots have a minimum turning radius on high adhesion surfaces due to lateral resistance R_y in eq. 7. Over small radial distances, the turning dynamics can be ignored since lateral motion is small. For longitudinal motion, the only nonlinearity is rolling resistance, which is small. Thus, the robots in Fig. 3 approximate radially confined point masses. If, instead, we allow unconstrained motion, lateral motion is overestimated compared to the nonlinear dynamics, and the system exhibits a prolonged decay to steady-state that is not present in the full nonlinear system. Thus, an unconfined point-mass model is less accurate than the confined model in representing the nonlinear dynamics near equilibrium.

Ignoring natural damping D for now, the radially confined system has nonlinear dynamics of the form

$$m\ddot{\mathbf{r}} = f_p(\mathbf{r}) - C\dot{\mathbf{r}} . \tag{11}$$

$\mathbf{r}$ is the vector of robot positions measured radially from the virtual leader, f_p is the vector of forces exerted by the APF controller on each robot as detailed above, C is a scalar damping coefficient that provides damping relative to absolute velocity and m is the mass of each robot. To linearize eq. 11, we find the partial derivatives of the total control force on any given robot with respect to the radial positions every other robot in the system. The magnitude of the total force on a single robot is

$$F_{tot} = \sum_{k=1}^{n-1} F_k(d_k)\cos(\gamma_k) + F_{vl}(r) . \tag{12}$$

k is the robot number relative to the robot under consideration., i.e., r_k is the position of the robot k robots away and $F_{vl}(r)$ is the force due to the virtual leader given by eq. 4 with $r = d_i$. Due to symmetry, the expression for F_{tot} is the same for each robot.

Let $j_k = \frac{\partial F_{tot}}{\partial r_k}|_{r_j = r_0 \forall j}$ and $j_0 = \frac{\partial F_{tot}}{\partial r}|_{r_j = r_0 \forall j}$ where r is the radial position of the robot under consideration. The Law of Cosines gives $d_k^2 = r^2 + r_k^2 - 2rr_k\cos(k\theta)$, the distance between two robots separated by k robots, for arbitrary r and r_k. $\cos(\gamma_k)$ is found from $r_k^2 = r^2 + d_k^2 - 2rd_k\cos(\gamma_k)$. Thus,

$$cos(\gamma_k) = \frac{r - r_k\cos(k\theta)}{\sqrt{r^2 + r_k^2 - 2rr_k\cos(k\theta)}} \tag{13}$$

Combining (12) with (13), differentiating with respect to r_k, and evaluating at the equilibrium distance r_0 gives

$$j_k = \frac{\alpha_d}{8}\frac{4r_0(1-\cos(k\theta)) + \sqrt{2}d_0\sqrt{1-\cos(k\theta)}(\cos(k\theta)-3)}{r_0^3(\cos(k\theta)-1)^2} \tag{14}$$

which is the change in the magnitude of the force on a robot due to the movement of a robot k robots away. The change in force on a robot resulting from movement of that robot is the sum of changes in force between it and each robot plus the change in force from the virtual leader

$$j_0 = \alpha_h\left(\frac{2h_0}{r_0^3} - \frac{1}{r_0^2}\right) + \sum_{k=1}^{n}\frac{\partial F_k}{\partial r}|_{r_0} = \frac{\partial F_{tot}}{\partial r} \tag{15}$$

where

$$\frac{\partial F_k}{\partial r}\bigg|_{r_0} = \frac{\sqrt{2}d_0\sqrt{1-\cos(k\theta)}(3\cos(k\theta)-1) - \alpha_d}{8}\frac{4r_0\cos(k\theta)(1-\cos(k\theta))}{r_0^3(\cos(k\theta)-1)^2} \tag{16}$$

The partial derivatives are assembled into Jacobian J describing the linearized relationship between each robot and the positions of all other robots in the system:

$$J = \begin{bmatrix} j_0 & j_1 & j_2 & \cdots & j_{n-1} \\ j_{n-1} & j_0 & j_1 & \ddots & j_{n-2} \\ j_{n-2} & j_{n-1} & j_0 & \ddots & j_{n-3} \\ \vdots & \ddots & \ddots & \ddots & \vdots \\ j_1 & j_2 & j_3 & \cdots & j_0 \end{bmatrix} = \begin{bmatrix} j_0 & j_1 & j_2 & \cdots & j_1 \\ j_1 & j_0 & j_1 & \ddots & j_2 \\ j_2 & j_1 & j_0 & \ddots & j_3 \\ \vdots & \ddots & \ddots & \ddots & \vdots \\ j_1 & j_2 & j_3 & \cdots & j_0 \end{bmatrix}$$

J is circulant due to rotational symmetry. Due to reflectional symmetry $j_i = j_{n-i} \forall 0 < i < n$, as the off-diagonal terms of J, defined in eq. 14 depend only on $\cos(k\theta)$, an even function of k. Thus, J is a symmetric circulant matrix whose properties we will make use of in the following sections. The linearized closed loop dynamics are found by replacing f_p in eq. 11 with J

$$m\ddot{\mathbf{r}} = J\mathbf{r} - C\dot{\mathbf{r}} . \tag{17}$$

Figure 4 compares the nonlinear system response under APF control to that of the linearized system eq. 17 for n = 5 robots and random initial conditions on each robot, showing that the linearized model is a reasonable approximation of the nonlinear dynamics near equilibrium.

V. Delay-Free Circular Equilibrium Stability

Figure 5 shows equilibrium states for $n = 6$ robots in formation around a virtual leader at the origin for three sets of control parameters. The robots start from random

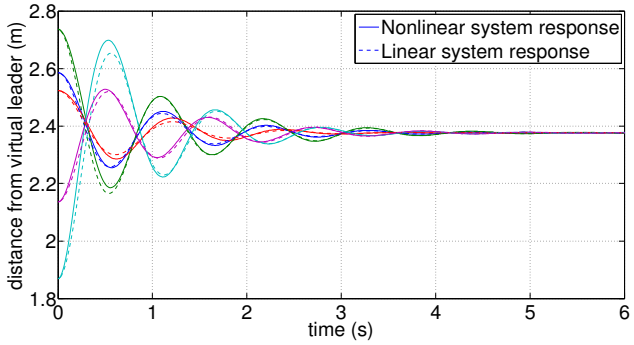

Figure 4. Comparison of nonlinear MIMO dynamics (solid lines) to linearized MIMO dynamics (dashed lines) for n = 5, α^* =1, h_0^* =1.

initial positions. In the Fig. 5a and (c), the circular equilibrium is unstable, while in (b), the desired equilibrium is stable. When the control parameters are too small, the control force from the virtual leader is weak compared to the intra-robot force and the equilibrium contracts, causing a robot's immediate neighbors to exert strong repulsive forces. The situation is analogous a mass suspended between two compressed springs, i.e., an unstable equilibrium; if perturbed, it will continue in the direction of perturbation. The same phenomenon exists in the system of robots when α^* and h_0^* are small. In order to avoid control parameters that cause this instability, we examine the eigenvalues of the radially confined system below.

The circular equilibrium is also unstable for large values of h_0^* and α^*, as in Fig. 5c. This instability is not described by the radially confined system because it arises as an unconfined point mass migrates tangentially about the equilibrium circle. In this case, the virtual leader repulsive force is strong and the configuration expands, resulting in strong attractive forces between adjacent robots. Although tangential motion is not possible for radially constrained nonholonomic robots, for other configurations, tangential motion is feasible. Therefore, this second instability regime must be avoided. We can determine parameters for which the desired equilibrium is tangentially unstable by examining the eigenvalues of the linearized system in which the robots are confined to move tangentially. This derivation is presented in [16] and thus is omitted here.

Figure 6 shows h_0^* and α^* needed to stabilize the circular equilibrium. Systems with few robots require smaller h_0^* and α^* for a stable equilibrium than do systems with many robots. In general, flexibility in choosing the control parameters diminishes as n increases. Analytical bounds on stability of the circular equilibrium are established by exploiting known properties of symmetric circulant matrices.

Theorem 2. *The largest eigenvalue γ_{max} of J (in an absolute sense) is the row sum of any row of J.*

Proof. The eigenvalues of a circulant matrix are [17]

$$\gamma_m = \sum_{k=0}^{n-1} c_k e^{j2\pi mk/n} \tag{18}$$

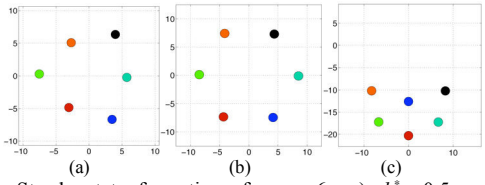

Figure 5. Steady state formations for $n=6$, a) $h_0^*=0.5$, $\alpha^*=1$, b) $h_0^*=1$, $\alpha^*=2$, and c) $h_0^*=1.5$, $\alpha^*=4$.

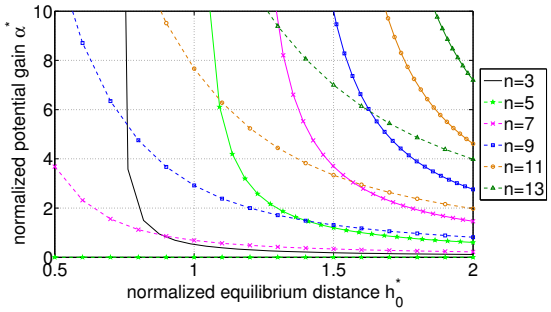

Figure 6. Control parameters needed to stabilize the circular equilibrium. Regions between the dashed and solid lines of the same color and symbol correspond to control parameters that result in a stable circular equilibrium.

where c_k are the elements of the first row of the circulant matrix, in this case J. Therefore, for m =0,

$$\gamma_0 = c_0 + c_1 + c_2 + \cdots + c_{n-2} + c_{n-1} = \sum_{k=0}^{n-1} c_k \tag{19}$$

is the row sum of any row of J. For all other $m>0$, $e^{j2\pi mk/n}$ has magnitude one but is complex. Because J is symmetric and real, all of its eigenvalues are real. Therefore, elements in eq. 18 with complex coefficients must cancel thus decreasing the overall magnitude of the eigenvalues. Therefore $\gamma_0 > \gamma_m \forall \ \ m \in (0,n)$.

Theorem 3. *The smallest eigenvalue γ_{min} of J (in an absolute sense) is*

$$\gamma_{min} = \begin{cases} \sum_{k=0}^{n-1} c_k (-1)^k & n \text{ even} \\ c_0 + 2\sum_{k=1}^{\frac{n-1}{2}} c_k \cos(\pi k/n)(-1)^k & n \text{ odd} \end{cases} \tag{20}$$

Proof. Examining eq. 18 for n even, the smallest eigenvalue is one for which $e^{j2\pi mk/n} = (-1)^k$. This occurs when $m = n/2$ since $e^{j2\pi \frac{n}{2}\frac{k}{n}} = (-1)^k$. Substituting this into (18) gives the expression in (20) for n even, which is the sum of even terms of the first row of J minus the sum of the odd terms of the first row of J. For n odd, let $m=(n-1)/2$, and $e^{j2\pi \frac{n-1}{2}\frac{k}{n}} = (-1)^k\left(\cos(\pi k/n) - j\sin(\pi k/n)\right)$. Since J is symmetric, $c_k = c_{n-k}$,

$$\gamma_{min} = c_0 + \sum_{k=1}^{\frac{n-1}{2}} c_k \left[(-1)^k \left(\cos(\pi \frac{k}{n}) - j\sin(\pi \frac{k}{n}) \right) + (-1)^{n-k} \left(\cos(\pi \frac{n-k}{n}) - j\sin(\pi \frac{n-k}{n}) \right) \right] \tag{21}$$

Since n is odd and $2k$ is even, $(-1)^{n-2k} = -1 \forall k$. Using this and trigonometric identities, (21) reduces to the expression in (21) for n odd.

Theorem 4. *The eigenvalues of the system in eq. 17 are $\mu_{i\pm} = -C/(2m) \pm \sqrt{\left(\frac{C}{m}\right)^2 - 4\frac{\gamma_i}{m}}\Big/2$ where γ_i are the eigenvalues of the Jacobian J.*

Proof. The state evolution matrix A is

$$A = \begin{bmatrix} 0_{n\times n} & I_{n\times n} \\ \frac{J}{m} & -\frac{C}{m} I_{n\times n} \end{bmatrix} \tag{22}$$

the eigenvalues of which are found by solving $0 = \det\left(\mu^2 I_{n\times n} + \mu C/m I_{n\times n} - J/m\right)$. The characteristic equation can be written explicitly in terms of γ_i [5]:

$$\det\left(\mu^2 I_{n\times n} + \mu\frac{C}{m} I_{n\times n} - \frac{J}{m}\right) = \prod_{i=1}^{n}\left(\mu^2 + \mu\frac{C}{m} - \gamma_i \frac{1}{m}\right)$$

This implies that the eigenvalues of A can be found by solving $0 = \mu^2 + \mu\frac{C}{m} - \gamma_i \frac{1}{m}$. Therefore,

$$\mu_{i\pm} = -\frac{C}{2m} \pm \frac{\sqrt{\left(\frac{C}{m}\right)^2 + 4\frac{\gamma_i}{m}}}{2} \tag{23}$$

μ_{i+} and μ_{i-} are the eigenvalues associated with γ_i.

Theorem 5. *The circular equilibrium is stable if $\gamma_{min} < 0$.*

Proof. For stability

$$\mu_{i+} = -\frac{C}{2m} + \frac{\sqrt{\left(\frac{C}{m}\right)^2 + 4\frac{\gamma_i}{m}}}{2} < 0 \tag{24}$$

Therefore, $\gamma_i < 0$ for stability.

As expected in a dissipative system, the stability of eq. 17 depends only on the eigenvalues of J and specifically on γ_{min}, the smallest eigenvalue of J. Taking theorems 3 and 5 together, we have shown that the circular equilibrium is stable for the system in eq. 17 if

$$0 > \begin{cases} \sum_{k=0}^{n-1} c_k(-1)^k & n \text{ even} \\ c_0 + 2\sum_{k=1}^{\frac{n-1}{2}} c_k \cos(\pi k/n)(-1)^k & n \text{ odd} \end{cases} \quad (25)$$

VI. Stability with Delay

Two sources of delay are considered: communication delay τ_{com} and on-board processing lag. Processing lag is delay due to local sensing τ_{samp}, during which sensor data are collected and a state estimate is computed, and delay due to control τ_{cnt}. τ_{com} is the time between when information is sent by one node and received by another. For a homogeneous fleet, communicated information is always delayed more than local information, since communicated information is processed on the sending robot prior to being sent and thus is already delayed by τ_{samp}. Control update on individual robots is time driven, while communication between robots is asynchronous. In the best case, communicated information is received just before a control update on the receiving robot. In Fig. 7, Robot B performs a control update, making use of new information from A, and applies the new control to its actuators at time *c* if communication is received by *c*. By the time it is used to update control on the receiving robot, communicated information is aged by $\tau_c = \tau_{com} + \tau_{samp} + \tau_{cnt}$. At worst, communicated data are received just after a control update at *c* and so will not be used until B has performed another complete sense-control cycle at *d* $(\tau_{cnt} + \tau_{samp})$ later, as in Fig. 7. Thus, the total elapsed time is $2\tau_{samp} + 2\tau_{cnt} + \tau_{com}$. The expected value of τ_c, the age of communicated data when used by the receiving robot, is $E(\tau_c) = E(\tau_{com}) + \frac{3}{2}(\tau_{samp} + \tau_{cnt})$. The delay of local information is always $\tau_p = \tau_{samp} + \tau_{cnt}$.

The linearized dynamics in eq. 17 subject to delays τ_c and τ_p are expressed by splitting A into A_u expressing undelayed dynamics, A_p encompassing dynamics related to τ_p, and A_c expressing dynamics related to communicated information:

$$\begin{bmatrix} \dot{\mathbf{r}} \\ \ddot{\mathbf{r}} \end{bmatrix} = A_u \begin{bmatrix} \mathbf{r} \\ \dot{\mathbf{r}} \end{bmatrix} + A_p \begin{bmatrix} \mathbf{r}(t-\tau_p) \\ \dot{\mathbf{r}}(t-\tau_p) \end{bmatrix} + A_c \begin{bmatrix} \mathbf{r}(t-\tau_c) \\ \dot{\mathbf{r}}(t-\tau_c) \end{bmatrix} \quad (26)$$

Since control is based on delayed information, $A_u = \begin{bmatrix} 0_{n\times n} & I_{n\times n} \\ 0_{n\times n} & 0_{n\times n} \end{bmatrix}$. The dependency of the potential function

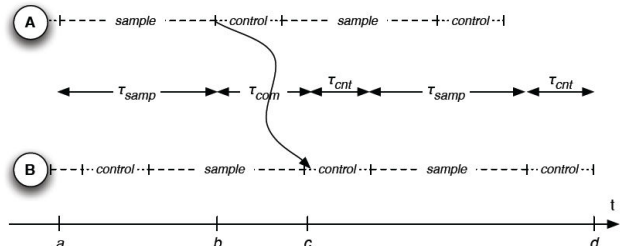

Figure 7. Communication timing: at time *a*, robot A samples its sensors. At *b* it has computed a state estimate and sends information to robot B, which receives it at *c* just before a control update (best-case) or just after a control update (worst-case), as shown.

force on each robot's knowledge of its own position is captured in the linearized system by j_0, the diagonal element of J, which is identical for each robot. The damping force depends only on each robot's own velocity. Therefore, A_p is

$$A_p = \begin{bmatrix} 0_{n\times n} & 0_{n\times n} \\ -\frac{K_0}{m} I_{n\times n} & -\frac{C}{m} I_{n\times n} \end{bmatrix}. \quad (27)$$

$K_0 = -j_0$ is the effective spring constant between each robot and ground. Each robot depends on the communicated position of the other robots via the APF controller. The control force exerted on each robot due to all other robots is captured in the linearized dynamics by the off diagonal elements of J:

$$A_c = \begin{bmatrix} 0_{n\times n} & 0_{n\times n} \\ -\frac{K_d}{m} & 0_{n\times n} \end{bmatrix} \quad (28)$$

$K_d = -J + diag(J)$ is the negative of the off diagonal elements of J, and *diag* returns the input matrix with everything but the main diagonal removed. K_d is interpreted as the stiffness matrix relating intra-robot forces to robot position.

In order to understand the stability characteristics of the delayed system eq. 26, we identify its characteristic equation and show that it can be divided into *n* independent factors. Consider the position of a single robot. The Laplace transformed position of robot i derived from eq. 26 is

$$R_i(s) = \frac{Q_i(s)}{|\, s^2 I_{n\times n} + s\frac{C}{m} e^{-s\tau_p} I_{n\times n} + \frac{K_0}{m} e^{-s\tau_p} I_{n\times n} + \frac{K_d}{m} e^{-s\tau_c} \,|} \quad (29)$$

where $Q_i(s)$ is a polynomial in s. The characteristic polynomial of the system is the same for all robots. Thus, the system poles are solutions to

$$0 = \left| \left(s^2 + (Cs + K_0)\frac{e^{-\tau_p s}}{m} \right) I_{n\times n} + \frac{K_d}{m} e^{-\tau_c s} \right| \quad (30)$$

Let $G = -\frac{K_d}{m} e^{-\tau_c s}$. Its eigenvalues are found by solving

$$0 = |\, \gamma I - G \,| = \prod_{i=1}^{n} (\gamma + \lambda_i \frac{e^{-\tau_c s}}{m}) \quad (31)$$

where λ_i are the eigenvalues of K_d. By letting γ in eq. 31 become $\left(s^2 + (Cs + K_0)\frac{e^{-\tau_p s}}{m} \right)$, (31) can be written:

$$0 = \prod_{i=1}^{n} \left(s^2 + (Cs + K_0)\frac{e^{-\tau_p s}}{m} + \frac{\lambda_i}{m} e^{-\tau_c s} \right) \quad (32)$$

Since K_d has n eigenvalues, the characteristic polynomial can be factored into n of these terms.

The stability of eq. 26 depends on the stability of each factor in eq. 32. Thus, we consider stability of the least stable factor. First, we consider $\tau_p = 0$ and $\tau_c > 0$, corresponding to a system with only communication delay. Recall that communicated data has aged by $\tau_c = \tau_{com} + \tau_{samp} + \tau_{cnt}$ when it is used on the receiving robot, and $\tau_p = \tau_{samp} + \tau_{cnt}$. Thus, $\tau_p \approx 0$ when $\tau_{com} >> \tau_{samp} + \tau_{cnt}$, i.e., local processing is fast compared with communication. The poles of a single factor of the characteristic equation are found by solving

$$0 = s^2 + \frac{C}{m}s + \frac{K_0}{m} + \frac{\lambda_i}{m}e^{-\tau_c s} \tag{33}$$

The maximum tolerable τ_c is the value for which the dominant poles of eq. 33 cross the imaginary axis. Let $s = -j\omega$ in eq. 33 and let τ_c^* be the threshold value of communication delay above which the system goes unstable. Then, from the magnitude condition,

$$\omega^2 = \frac{2K_0 m - C^2}{2m^2} + \frac{1}{2m^2}\sqrt{C^4 - 4C^2K_0 m + 4\lambda_i^2 m^2} \tag{34}$$

gives ω at which the poles of the factor cross into the right half plane, which does not depend on τ_c^*. Also, the poles corresponding to the factor with $\lambda_i = \lambda_{max}$, the largest eigenvalue of K_d, cross highest up on the imaginary axis.

The angle contribution of the complex exponential reduces to $\angle e^{-\tau_c s} = -\tau_c\omega$. Substituting $j\omega$ for s in (33), and finding the smallest value of τ_c^* that satisfies the angle condition gives the maximum tolerable τ_c as

$$\tau_c^* = \frac{1}{\omega}\left[\pi - \tan^{-1}\left(\frac{\omega C}{K_0 - m\omega^2}\right)\right] \tag{35}$$

where ω is given by eq. 34.

Next, we identify λ_i for which τ_c^* is smallest. The eigenvalues of K_d are closely related to the eigenvalues of J since $K_d = -J + diag(J)$. Recall from eq. 18 that the eigenvalues of a circulant matrix are weighted sums of the elements of the first row of the matrix. In eq. 18, the weight of the first element is always unity. Since the first row of $-K_d$ is the first row of J with the first element removed, the eigenvalues of K_d are the eigenvalues of $-J$ minus K_0. Therefore, by extension of theorems 1 and 2, the maximum and minimum eigenvalues of K_d are

$$\lambda_{max} = \sum_{k=1}^{n-1} c_k \tag{36}$$

$$\lambda_{min} = \begin{cases} \sum_{k=1}^{n-1} c_k(-1)^k & n \text{ even} \\ 2\sum_{k=1}^{\frac{n-1}{2}} c_k \cos(\pi k/n)(-1)^k & n \text{ odd} \end{cases} \tag{37}$$

Figure 8 shows how eq. 35 varies with the magnitude of λ_i, the eigenvalues of K_d. Eq. 35 decreases monotonically as $|\lambda_i|$ increases. This implies that the eigenvalue of K_d with the lowest associated value of τ_c^* is one of the extreme values of λ_i, namely either λ_{min} or λ_{max}. In general, $\lambda_{max} > 0$, $\lambda_{min} < 0$ and $|\lambda_{max}| > |\lambda_{min}|$ (this can be seen by comparing eq. 36 and 37). Due to the shape of eq. 35, then, the system will go unstable at the value of τ_c^* corresponding to λ_{max}. Therefore, stability of the system with communication delay depends on the maximum eigenvalue of K_d.

Figure 8b compares the analytical stability bound for tolerable delay given by eq. 35 to the settling time of a series of simulations of the nonlinear system subject to communication delay. For sets of control gains shown, eq. 35 accurately predicts the value of τ_c at which the system goes unstable. The upper and lower simulation curves, respectively, denote the mean 2% settling time of all robots in the system plus and minus the standard deviation in settling time among all robots. An interesting feature of Fig. 8a is the region for small $|\lambda|$ in which τ_c^* does not exist, implying that when all eigenvalues of K_d are in this region, the system will not go unstable due to τ_c. The boundaries of this region are derived by considering that when ω in eq. 34 becomes complex, a real value of τ_c^* no longer exists. This occurs when $0 > C^4 - 4C^2K_0 m + 4\lambda_i^2$. Since $|\lambda_{max}| > |\lambda_{min}|$, if

$$\lambda_{max} < C\sqrt{\frac{K_0}{m} - \frac{C^2}{4m^2}} \tag{38}$$

the system will not go unstable due to communication delay. The system can tolerate unbounded communication delay because the force due to the virtual leader is not delayed. If the virtual leader is strong enough even as communication delay increases, the system can still be stable. However, the force due to the virtual leader is subject to processing delay hence the system will go unstable if the processing delay is large enough. The selection of parameters such that eq. 38 is satisfied is considered in [16].

Next, we consider the case where communication is fast compared with on-board processing, i.e., $\tau_{com} << \tau_{samp} + \tau_{cnt}$ and thus $\tau_c \approx \tau_p > 0$. The factors of the characteristic polynomial of the system can be rewritten

$$0 = \prod_{i=1}^{n}\left(s^2 + (Cs + K_0 + \lambda_i)\frac{e^{-\tau_p s}}{m}\right) \tag{39}$$

As before, for the overall system to be stable, each factor must be stable. Consider a single factor in isolation:

$$-1 = \frac{(Cs + \lambda_i + K_0)e^{-\tau_p s}}{ms^2} \tag{40}$$

The above equation satisfies the magnitude and angle conditions when evaluated at its poles. First consider the magnitude condition. We are interested in determining the values of τ_p at which the poles of the factor cross the imaginary axis. Letting $s = j\omega$ and solving the magnitude condition for ω gives

$$\omega^2 = \frac{C^2}{2m^2} + \frac{1}{2m^2}\sqrt{C^4 + 4m^2(\lambda_i + K_0)^2}\,. \tag{41}$$

We evaluate the angle condition at the point where the poles cross the imaginary axis by letting $s = j\omega$ in order to find the critical value of τ_p, which we denote τ_p^* as

$$\tau_p^* = \frac{1}{\omega}\tan^{-1}\left(\frac{C\omega}{\lambda_i + K_0}\right) \tag{42}$$

where ω is given in eq. 42. Figure 9a shows τ_p^* as a function of λ_i. The smallest value of τ_p^* corresponds to one of the extreme values of λ_i (either λ_{min} or λ_{max}). Since $|\lambda_{max}| > |\lambda_{min}|$, by examining Figure 9a, we deduce that the smallest τ_p^* will correspond to λ_{max}. Therefore the stability of the system with respect to τ_p also depends on the maximum eigenvalue of the Jacobian.

Figure 9b compares the analytical stability bound given by eq. 42 and settling time measurements from a series of simulations of the nonlinear system in which the robots are subject to increasing local delay τ_p. Upper and lower simulation curves denote the mean 2% settling time plus and minus the standard deviation in settling time. For both sets of control gains shown, eq. 42 accurately predicts the value of τ_p at which the simulated system goes unstable.

There are important differences between the τ_p and τ_c stability criteria defined in eqs. 43 and 35, respectively. First, the system tends to go unstable for much smaller values of τ_p than of τ_c indicating that the system is more sensitive to local delay than to communication delay. This makes sense since all information whether computed locally or communicated between robots is subject to processing

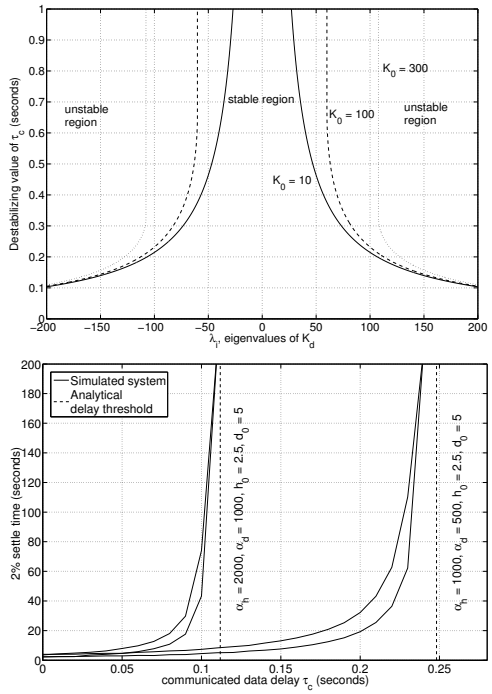

Figure 8. (a) Destabilizing value of communication delay τ_c^* as a function of the eigenvalues of K_d for three values of K_0, (b) Comparison of analytical stability threshold for τ_c with simulation of the non-linear multi-robot system for $\tau_n = 0$.

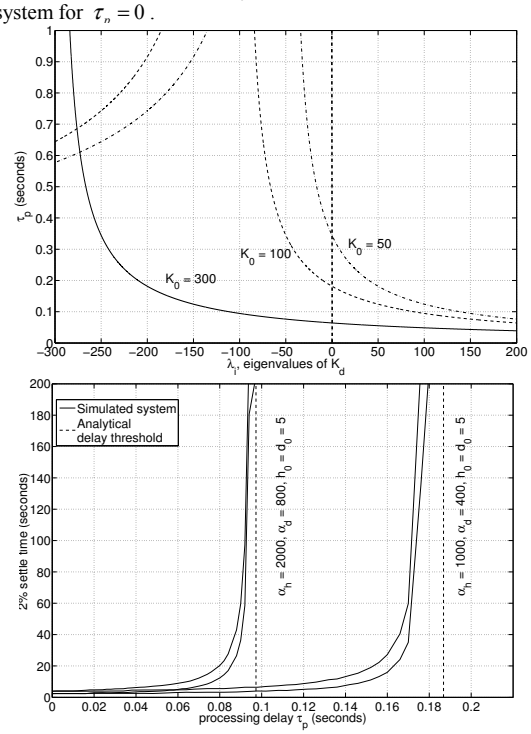

Figure 9. (a) Destabilizing value of processing delay τ_p^* as a function of the eigenvalues of K_d for three values of K_0. (b) Comparison of analytic stability threshold with simulation of the nonlinear multi-robot system for $\tau_p = \tau_c$.

delay while only communicated information is affected by communication delay. While τ_c^* increases with increasing K_0, τ_p^* decreases with increasing K_0. These trends indicate that while communication delay might be partially compensated for by increasing α_h, doing so will make the system more sensitive to processing delay. Finally, there is no region for which the system will not go unstable at some value of τ_p. Instability associated with each type of delay depends on the largest eigenvalue of K_d. Moreover, making λ_{max} as small as possible increases the system's tolerance to both types of delay. However, by comparing the region near the origin in Fig. 8a and 9a, it can be seen that τ_p^* is less sensitive to reductions in λ_{max} than is τ_c^*.

VII. Experimental Evaluation

In order to test the accuracy of the theoretical analysis, we performed a series of experiments with $n = 4$ Dynabots arranged in a circular formation as in Fig. 3. The Dynabots were moved 1.0m back from their equilibrium positions to represent a perturbation from the circular equilibrium and were commanded to converge to equilibrium autonomously under APF control. Local processing delay was changed between runs by introducing an artificial delay between when state information was computed and when it was used to update control. The artificial delay was implemented using a state data queue. By adjusting the size of the queue, the processing delay is adjusted in increments of the control interval, which is 50ms. Figure 10 shows sample results for local delay from $\tau_p = 0.025$ to 0.225 sec. A run was stopped after the robots had visually "settled" or when it was clear the system was unstable. The settling time of each robot is estimated (except for Fig. 16c which is unstable). Clearly, the settling time increases with processing delay.

[16] presents analytic approximations to settling time for each type of delay, derived from the characteristic equation eq. 30 using a Pade approximation of the delay function. Settling time depends on the magnitude of the real part of the dominant pole and its residue. At one extreme, when a dominant pole is far from all other poles, its residue is unity and its response envelope is $e^{-\zeta\omega_n t}$ where $\zeta\omega_n$ is the real part of the pole. The other extreme is the case of a root of multiplicity, with decay envelope $te^{-\zeta\omega_n t}$, with $te^{-\zeta\omega_n t} > e^{-\zeta\omega_n t}$ for $t > 1$. For poles between these, the decay response falls between these two bounds. [16] uses $te^{-\zeta\omega_n t}$ and $e^{-\zeta\omega_n t}$ as the upper-and lower-bound response envelopes, respectively, where $\zeta\omega_n$ is the real part of the dominant pole pair of the factor corresponding to λ_{max}. Choosing $te^{-\zeta\omega_n t}$ as the upper-bound is important since there can be roots of multiplicity due to symmetry; the longest decay response would belong to the root of multiplicity closest to the imaginary axis.

The 2% settling time fluctuates between $3/\zeta\omega_n$ and $4/\zeta\omega_n$ for $\zeta < 0.8$ [18]. Therefore, the lower bound on settling time is taken as $t_s \approx 3/\zeta\omega_n$. The 2% settling time of $te^{-\zeta\omega_n t}$ is the solution to $0.02 = t_s e^{-\zeta\omega_n t_s}$ which is solved using the -1 branch of the Lambert W function. [16] derives approximations of $\zeta\omega_n$ for each delay case. It is possible to validate these analytic approximations using experimental data and at the same time evaluate analytic stability bounds. First, the effective damping coefficient is adjusted to include both the natural viscous damping, which is measured for the Dynabots on asphalt as $D = 3\,\text{N/m/s}$ [16] and the effective damping due to rolling resistance. Rolling resistance, while not viscous, is dissipative in nature. The viscous damping coefficient D is modified to take into account the nonlinear rolling resistance and to provide an effective damping term. Neglecting rolling resistance, the equivalent steady state velocity is reached for the system if the damping is taken as $D^* = F_a / v_{xss}$ where v_{xss} is the steady state velocity and F_a is the applied force from the wheels, which can be

approximated directly from the wheel torque measurements. Data were recorded from a Dynabot driven straight on asphalt at a steady velocity similar to the speeds reached by the Dynabots during the stability tests in Fig. 10. The steady-state velocity and force were recorded, and the equivalent damping coefficient is $D^* \approx 10$ N/m/s. The predicted settling time bounds are computed with this value of natural damping and control parameters used in Fig. 10. The results in Fig. 11 show that settling time bounds measured from experimental data fall within analytic approximations to settling time bounds, and asymptotic stability bounds match predicted values quite well for control parameter sets used in experiments.

VIII. Conclusions

We have demonstrated the existence of a circular equilibrium for a fleet of robots coming into formation about a virtual leader under potential function control. We have derived bounds on the control parameters necessary to guarantee that this equilibrium is stable, when robots assume a radial pose. Either communication or local processing delay can result in instability. We derive exact stability bounds for each delay and show that while local processing delay can always cause instability, given the right control parameters, the system can tolerate infinite communication delay. Analytic stability bounds are validated through experiments with a system of four Dynabots.

The present examination is limited to regulation of a specified equilibrium and pose and a clear next step would be to extend these results to more general equilibrium states and tracking. Such generalization would not only destroy symmetry, it would also excite the turning dynamics of the nonholonomic robots, making the problem much more challenging to address.

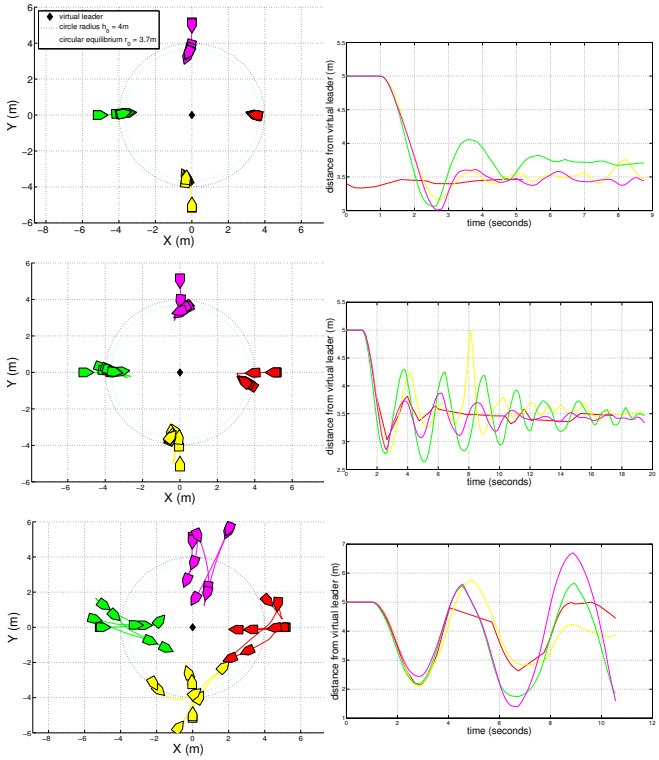

Figure 10. Trajectories (top) and history of estimated distance from virtual leader (bottom) for experimental stability test with four Dynabots about a circular equilibrium, α_h=1500, α_d=1500, h_0 = 4m, d_0 = 5m, $C = 20$ N/m/s. (a) $\tau_p \approx 0.025$ s, the Dynabot's natural delay due to state estimation and control, (b) $\tau_p \approx 0.12$ s, (c) $\tau_p \approx 0.225$ s.

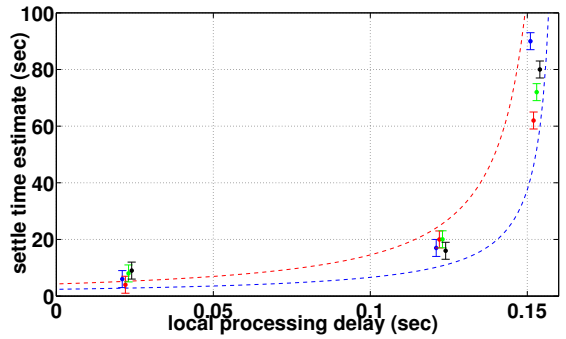

Figure 11. Measured settling times compared to lower and upper analytic bounds from [16] for natural damping $D* = 10$ N/m/s.

References

[1] Munawar, K. and Uchiyama, M. (1997). Slip compensated manipulation with cooperating multiple robots. *Proc. of the 36th Conference on Decision and Control, San Diego, CA*, **2**: 1918–1923.

[2] Bachmayer, R. and Leonard, N.E. (2002). Vehicle networks for gradient descent in a sampled environment. *Proc. of the 41st IEEE Conf. on Decision and Control*, **1**: 112-117.

[3] Wu, Z., Guan, Z., Wu, X., and Li, T. (2007). Consensus based formation control and trajectory tracing of multi-agent robot systems. *J. Intelligent and Robotic Systems*, **48**: 397–410.

[4] Ren, W. and Atkins, E. M. (2005). Second-order consensus protocols in multiple vehicle systems with local interactions. *AIAA Guidance, Navigation, and Control Conference*.

[5] Olfati-Saber, R. and Murray, R.M. (2004). Consensus problems in networks of agents with switching topology and time-delays. *IEEE Transactions on Automatic Control*, **49**(9):1520–1533.

[6] Tanner, H.G., Pappas, G.J., and Kumar, V. (2004). Leader-to-formation stability. *IEEE Trans. on Robotics and Automation*, **20**(3): 443–455.

[7] Fiorelli, E.A. (2005). Cooperative Vehicle Control, Feature Tracking and Ocean Sampling. *PhD thesis*, Princeton University.

[8] Leonard, N.E. and Fiorelli, E. (2001). Virtual leaders, artificial potentials and coordinated control of groups. *Proc. of the 40th IEEE Conf. on Decision and Control*, **3**: 2968–2973.

[9] Ögren, P., Fiorelli, E., and Leonard, N. E. (2002). Formations with a mission: Stable coordination of vehicle group maneuvers. *Proc. Symp. on Mathematical Theory of Networks and Systems*, 12-16.

[10] Chen, Y.Q. and Wang, Z. (2005). Formation control: A review and a new consideration. *Proc. IEEE Int. Conf. on Intelligent Robots and Systems*, 3181–3186, 2-6 Aug.

[11] Liu, X., Goldsmith, A., S.S. Mahal, and Hedrick, J.K. (2001). Effects of communication delay on string stability in vehicle platoons. *IEEE Intelligent Transportation Systems Conf. Proc.*, 625–630, 25-29.

[12] Bliman, P.A., Ferrari-Trecate, G. (2008) Average consensus problems in networks of agents with delayed communications. *Automatica* doi:10.1016/j.automatica.2007.12.010, in press.

[13] Koren, Y. and Borenstein, J. (1991). Potential field methods and their inherent limitations for mobile robot navigation. *Proc. Int. Conf. on Robotics and Automation*, **2**: 1398–1404.

[14] Murphy, J.P., Wachter, L.M., and Ray, L., (2007). Computational Resource Allocation in Cooperative Control of Mobile Robots, RoboComm, *First Int. Conf. on Robot Communication and* Coordination.

[15] Wachter, L., Murphy, J., and Ray, L. (2008) Potential Function Control for Multiple High-Speed Nonholonomic Robots, Int.l Conference *on Robotics and Automation, video*.

[16] Wachter, L. Design of a Motion Coordination Architecture for a Multi-Robot System with Hardware Constraints, M.S. Thesis, Thayer School of Engineering, Dartmouth College, June 2008.

[17] Rojo, O. and Rojo, H. (2004). Some results on symmetric circulant matrices and on symmetric centrosymmetric matrices. Linear Algebra and its Applications, **392**:211–233.

[18] Ogata, K. (2002). *Modern Control Engineering*. Prentice Hall, 4th ed.